

## CHEMICAL, RADIATIVE, AND DILUTIVE EFFECTS OF CO<sub>2</sub> ADDITION ON SOOT FORMATION IN JET A-1 KEROSENE CO-FLOW DIFFUSION FLAME

by

**Yu YANG<sup>a,b</sup>, Qing LI<sup>a\*</sup>, Jiajian ZHU<sup>a</sup>, and Bo ZHOU<sup>c</sup>**

<sup>a</sup> College of Aerospace Science and Engineering,  
National University of Defense Technology, Hunan, China

<sup>b</sup> National Engineering Research Center of New Energy Power Generation,  
North China Electric Power University, Beijing, China

<sup>c</sup> Department of Mechanics and Aerospace Engineering,  
Southern University of Science and Technology, Shenzhen, China

Original scientific paper

<https://doi.org/10.2298/TSCI220604136Y>

*With the development of aviation industry, it is urgently to investigate the soot formation properties of aviation kerosene to better control the soot emissions. The dilutive, chemical and radiative effects of CO<sub>2</sub> on the soot inception, condensation and hydrogen abstraction acetylene addition (HACA) growth processes in laminar co-flow Jet-A1 kerosene diffusion flames were numerically investigated by employing detailed chemical mechanisms and soot sectional models. The results showed that the addition of CO<sub>2</sub> dramatically decreased the maximum temperature (by 92 K) and soot volume fraction (by 41.0%). The dilutive effect of CO<sub>2</sub> contributed the most to the decrease of temperature and soot volume fraction. It also was the main factor in the decrease of soot inception, condensation and HACA growth processes. The chemical effect of CO<sub>2</sub> had little impact on the decomposition of fuels into light hydrocarbons, but obviously limited the growth of light hydrocarbons to A1. The radiative effect of CO<sub>2</sub> decreased the maximum temperature and soot volume fraction by 13 K and 5.2% (from 1.92-1.82 ppm). It had little impact on the soot inception, condensation and HACA growth rates.*

Key words: Jet A-1 kerosene diffusion flame, CO<sub>2</sub> addition, chemical effect, radiative effect, soot inception

### Introduction

Recently, soot emission has received considerable attention since it increases the risk of respiratory and cardiovascular diseases for humans and intensifies the greenhouse effect [1]. It is reported that soot emission is mainly attributed to the use of hydrocarbon fuels, such as gasoline and kerosene [2]. With the development of the aviation industry [3, 4], it is urgently to investigate the soot formation properties of kerosene to better control the soot emissions.

Many researchers have experimentally and theoretically studied the soot formation properties in aviation kerosene combustion. The soot formation was described by the soot inception, condensation, HACA (the hydrogen abstraction acetylene addition) surface growth mechanism and soot oxidation [5]. Among them, the soot inception was the initial process and considered the dominant role in the soot formation processes [6]. Sun *et al.* [7] experimentally

\* Corresponding author, e-mail: qing.li@nudt.edu.cn

compared the soot formation properties of RP-3 kerosene with that of *n*-dodecane diffusion flames. They found that the primary particle diameter of *n*-dodecane was smaller than that of RP-3 since the soot inception was enhanced in RP-3 flame. Saffaripour *et al.* [8] considered the four-rings pyrolytic aromatic hydrocarbons (A4) as the soot inception precursors for a laminar co-flow Jet-A1 flame. The results showed the modified model was able to predict soot size distributions and structure well comparing with the experimental results. Besides the soot inception, the influence of different chemical mechanisms on the soot condensation in a RP-3 kerosene co-flow diffusion flame was studied by Sun *et al.* [9]. They found that the C14 *n*-alkanes mechanism had little effect on the prediction of soot condensation. Abdalla *et al.* [10] experimentally studied the influence of flow rates on the soot oxidation rate in an inverse RP-3 inverse flame. The results showed that a higher flow rate resulted in a larger amount of volatile organic compounds [11], leading to an increase in the reactive sites for the oxidizer.

Previous studies have comprehensively revealed the soot formation process in the combustion of aviation kerosene at the atmospheric condition. In the ground experiment, the combustion of hydrocarbon fuels was widely used to obtain the high enthalpy air-flow, which produces substantial amounts of contaminating species, such as CO<sub>2</sub> and H<sub>2</sub>O [12, 13]. The contaminations were proved to have a great impact on the combustion characteristics of aviation kerosene [14]. Liang *et al.* [15] found that the ignition delay time of RP-3 was inhibited with 10% CO<sub>2</sub> addition at temperatures below 1300 K. The CO<sub>2</sub> addition decreased the formation rate of OH and O radicals through the reactions of CO<sub>2</sub> + O = O<sub>2</sub> + CO and CO<sub>2</sub> + OH = CO + HO<sub>2</sub>, leading to a suppression effect on the ignition of aviation kerosene. Wang *et al.* [16] experimentally studied the effect of CO<sub>2</sub> on aviation kerosene supersonic combustors. The results showed that the addition of CO<sub>2</sub> reduced the wall pressure by increasing the heat capacities, especially at the equivalence ratio of 0.73. Li *et al.* [17] found that CO<sub>2</sub> had a non-linearly reduced influence on the wall pressure in an aviation kerosene supersonic combustion. In addition, they concluded that CO<sub>2</sub> resulted in the decrease of combustion efficiency and streamwise impulse. Previous studies mainly focused on investigating the effect of the CO<sub>2</sub> contamination on the ignition delay time, combustion pressure and efficiency in the aviation kerosene combustion. So far, however, there is much less information about the effect of CO<sub>2</sub> contamination on soot formation in the aviation kerosene flames.

To date, there were several investigations exploring the effect of CO<sub>2</sub> addition on the soot formation in light-hydrocarbon-fueled flames, such as CH<sub>4</sub> and C<sub>2</sub>H<sub>4</sub>. A numerical analysis was presented to study the formation of soot in CH<sub>4</sub>/air co-flow diffusion flames with different CO<sub>2</sub> dilutive ratios [18]. It was observed that the soot loading reduced with the increased CO<sub>2</sub> fraction. A similar trend can be found in a C<sub>2</sub>H<sub>4</sub>/air co-flow diffusion flame with CO<sub>2</sub> addition [19]. To comprehensively reveal the chemical and dilutive effects of CO<sub>2</sub> on the soot formation, the fictitious CO<sub>2</sub> as a substitute for the real CO<sub>2</sub> was proposed by Liu *et al.* [20]. They found the reactions CO<sub>2</sub> + H = CO + OH and CO<sub>2</sub> + CH = HCO + CO were responsible for the chemical effect of CO<sub>2</sub> addition. Guo and Smallwood [19] found that the chemical effect of CO<sub>2</sub> reduced the concentration of H radical, which consequently decreased the soot inception and soot surface growth rates. However, the chemical effect of CO<sub>2</sub> on soot oxidation was negligible [19]. In addition to the chemical and dilutive effects, the radiative effect cannot be ignored [21, 22]. Liu *et al.* [23] reported that the radiative effect of H<sub>2</sub>O lowered the temperature in the centerline region by 12 K. Considering the Planck mean absorption coefficients of CO<sub>2</sub> at temperatures above 500 K were larger than those of H<sub>2</sub>O [24], it is necessary to explore the radiative effect of CO<sub>2</sub> on the soot formation in the aviation kerosene combustion.

The aim of this paper was to numerically investigate the different effects of CO<sub>2</sub> addition on the air-flow on the soot formation in a laminar co-flow Jet-A1 kerosene diffusion flame. The fictitious CO<sub>2</sub> was introduced to isolate the chemical, dilutive and radiative effects. Detailed soot sectional model and chemical mechanism were adopted to analysis the different effect of CO<sub>2</sub> on the soot formation processes. This study firstly and comprehensively revealed the chemical, dilutive and radiative effects of CO<sub>2</sub> addition on soot nucleation, condensation and HACA surface growth in the aviation kerosene flame, which provided a theoretical basis for developing soot emissions-reduction schemes in aviation kerosene combustion.

### Computational details

The laminar co-flow Jet A-1 kerosene diffusion flames were simulated in the Yale burner [8], which has an inner diameter of 11 mm and 102 mm for the fuel tube and the concentric annular air tube, respectively. The *n*-decane (C<sub>10</sub>H<sub>22</sub>), *n*-propylcyclohexane (C<sub>9</sub>H<sub>18</sub>), and *n*-propylbenzene (C<sub>9</sub>H<sub>12</sub>) were regarded as the surrogates for the Jet A-1 kerosene [8]. The flow rates of the fuels were set as 23.5 cm per second referring to [8] in all cases. The inlet air velocity was set as 20.1 cm per second in Case 1 but 23.1 cm per second in cases 2-4 since 15 vol.% CO<sub>2</sub> or fictitious CO<sub>2</sub> was added to the air-flow. The inlet temperature of fuel and air-flows were 473 K and 423 K. The mole fractions of species in the fuel and air-flows are listed in tab. 1.

As shown in tab. 1, four different cases were simulated. To isolate the chemical, radiative and dilutive effects of CO<sub>2</sub> on the flame properties, two fictitious species F<sub>1</sub>CO<sub>2</sub> and F<sub>2</sub>CO<sub>2</sub> were introduced. Both species had the same transport and thermochemical properties as real CO<sub>2</sub>. The F<sub>1</sub>CO<sub>2</sub> was allowed to participate in radiation but was chemically inert, and F<sub>2</sub>CO<sub>2</sub> was both chemically and radiatively inert. Comparisons between Cases 1 and 2 containing all the effects of CO<sub>2</sub> addition. Cases 2 and 3 were compared to isolate the chemical effect of CO<sub>2</sub>, while the radiative effect of CO<sub>2</sub> was quantified through a comparison between Cases 3 and 4. Moreover, the dilutive effect of CO<sub>2</sub> addition was obtained by comparing the results of Cases 1 and 4.

**Table 1. The mole fractions of species in the fuel and air-flows**

Case	Fuel flow				Air-flow				
	C <sub>10</sub> H <sub>22</sub>	C <sub>9</sub> H <sub>18</sub>	C <sub>9</sub> H <sub>12</sub>	N <sub>2</sub>	O <sub>2</sub>	N <sub>2</sub>	CO <sub>2</sub>	F <sub>1</sub> CO <sub>2</sub>	F <sub>2</sub> CO <sub>2</sub>
1	0.0345	0.0055	0.01	0.95	0.25	0.75	0	0	0
2	0.0345	0.0055	0.01	0.95	0.23	0.68	0.09	0	0
3	0.0345	0.0055	0.01	0.95	0.23	0.68	0	0.09	
4	0.0345	0.0055	0.01	0.95	0.23	0.68	0		0.09

The computational domain was 3.78 cm (radial direction,  $-r$ )  $\times$  11.56 cm (streamwise direction,  $-z$ ) with 80 ( $-r$ )  $\times$  160 ( $-z$ ) control volumes. Non-uniform grids were used and the minimal spatial resolutions of the mesh were 0.2 mm and 0.3 mm in the radial and streamwise directions, respectively. It was checked that further refinement of the mesh did not result in any change in the results. When the maximum relative variation of soot volume fraction (SVF) over 100 iterations was less than  $1 \cdot 10^{-4}$ , iterations were considered as converged.

### Numerical models

The flame code developed by Eaves *et al.* [25] was used in this study. A detailed soot sectional model [23] was adopted. Soot formation processes including soot inception, condensation, surface growth and oxidation were considered at each section. Soot inception was modeled by the collision of two pyrenes (A4) [26]. The HACA mechanism was adopted to described

the soot surface growth and oxidation. The fraction of reactive soot surface sites  $\alpha$  was an empirical parameter and was assumed as  $\alpha = 0.03$  to ensure that the simulation results matched the experimental results. The condensation process was modeled by the collision between the soot and the A4. The condensation efficiency  $\gamma$  which describes the probability of sticking was set as 0.5 [6]. More computational details can be found in [25].

The chemical mechanism developed by Saffaripour *et al.* [8] was introduced in this study. The radiative properties of CO<sub>2</sub>, H<sub>2</sub>O were obtained via the statistical narrow-band correlated-k method with 9 bands ranging 150-9300 cm<sup>-1</sup>. The Rayleigh expression [27] was adopted to calculate the absorption coefficient of soot. The discrete ordinate method with T3 quadrature scheme [28] was used to solve the radiative transfer equation.

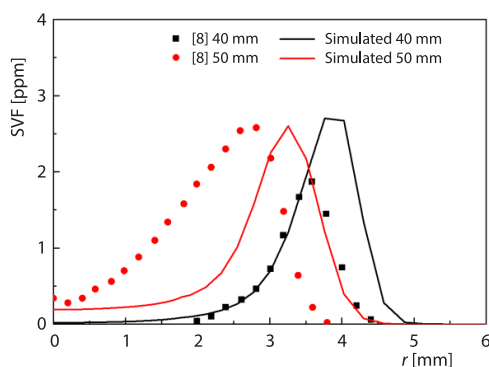


**Figure 1.** The comparison of simulated and experimental radial profile of SVF at heights of 40 and 50 mm

were attributed to oversimplified soot inception model [29], which was assumed to be the collision of two A4. Generally, the models used in this study were validated for modelling co-flow diffusion Jet A-1 kerosene flames.

## Results and discussion

### *The effects of CO<sub>2</sub> on temperature*

Simulated 2-D temperature distributions and peak temperatures of all cases were compared in fig. 2. In figs. 2(a) and 2(b), the addition of 15 vol.% CO<sub>2</sub> had a significant suppression effect on the peak temperature (by 92 K). In addition, the flame was lifted by around 10 mm in Case 2 since the CO<sub>2</sub> addition led to a longer ignition delay time. The dilutive effect of CO<sub>2</sub> addition also caused an obvious drop in the maximum temperature by 70 K, as shown in figs. 2(a) and 2(d).

The radiative and chemical effects of CO<sub>2</sub> addition resulted in a modest drop in the maximum temperature by 13 K, figs. 2(c) and 2(d), and 9 K, figs. 2(b) and 2(c), respectively. The radiative effect of CO<sub>2</sub> on the drop of temperature was due to high radiation ability of CO<sub>2</sub>, which resulted in high radiative heat loss. In addition, a lifted distance of 10 mm can also be observed in Cases 3 and 4 shown in figs. 2(c) and 2(d).

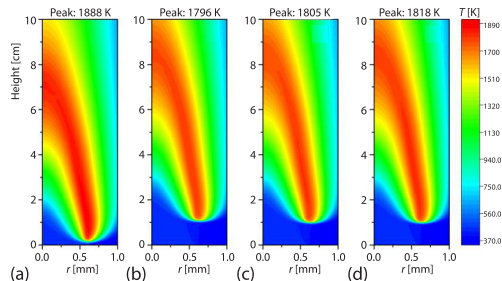


**Figure 2.** The temperature distributions of (a) Case 1, (b) Case 2, (c) Case 3, and (d) Case 4

### Validation of models

To validate the models used in this study, the simulated radial profile of SVF at heights of 40 and 50 mm in Case 1 were compared with the experimental results introduced from [8]. As shown in fig. 1, the simulated SVF first increased and then decreased with the increase of radius at heights of 40 and 50 mm, agreed well with those of experimental SVF. The maximum simulated SVF at height of 40 mm was 2.7 ppm larger than that of experimental SVF (1.9 ppm). At height of 50 mm, both the maximum simulated and experimental SVF were 2.6 ppm. The discrepancies between the experimental and simulated results

### The effects of CO<sub>2</sub> on soot formation

The SVF distributions of four different flames were presented in fig. 3. It can be seen from figs. 3(a) and 3(b) that the soot formation was greatly suppressed by the total effect of CO<sub>2</sub> addition (includes chemical, diluted and radiative effects), with the maximum SVF decreased from 2.9-1.71 ppm (by 41.0%). In fig. 3(a) and 3(d), the dilutive effect of CO<sub>2</sub> decreased the maximum SVF by 0.98 ppm (by 33.85%), which contributed the most to the drop of SVF compared to the radiative and chemical effects. The reason was that the dilutive effect markedly lowered flame temperature shown in fig. 2. The radiative effect of CO<sub>2</sub> lowered the maximum SVF from 1.92 ppm in fig. 3(d) to 1.82 ppm in fig. 3(c), with a drop of 5.2%. This could be explained by the decrease of temperature caused by the radiative heat loss of CO<sub>2</sub>. The chemical effect of CO<sub>2</sub> resulted in a decline of maximum SVF by 0.11 ppm (by 6.0%), depicted in figs. 3(c) and 3(d). As mentioned previously, the soot formation including soot inception, condensation and HACA surface growth. To comprehensively reveal different effects of CO<sub>2</sub> on different soot formation processes, the soot inception, condensation and HACA surface growth rates at the heights of 0.5, 1.5, and 3.0 cm in Case 1 were discussed following. Since the flames were lifted around 10 mm in Cases 2-4, the results at heights of 1.5, 2.5, and 4.0 cm for Cases 2-4 were compared with those at heights of 0.5, 1.5 and 3.0 cm in Case 1. It was noted that the heights indicated hereinafter refer to those in Case 1.

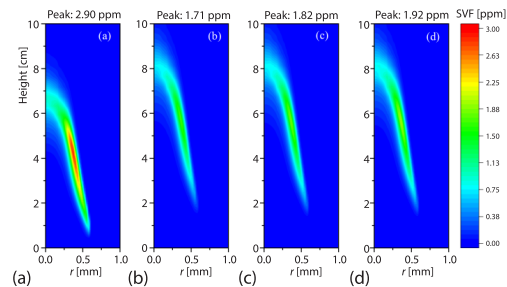


Figure 3. The SVF distributions of (a) Case1, (b) Case 2, (c) Case 3, and (d) Case 4

### The effect of CO<sub>2</sub> on soot inception

As shown in fig. 4, the soot inception mainly happened at the lower region of the flame. The inception rates at height of 0.5 cm were obviously larger than those at heights of 1.5 cm and 3.0 cm. The differences in soot inception rates among the four cases at heights of 1.5 cm and 3.0 cm were quite modest. While at height of 0.5 cm, the CO<sub>2</sub> addition caused the maximum inception rate falling from  $4.8 \cdot 10^{-5}$  g/cm<sup>3</sup> per second (Case 1) to  $2.3 \cdot 10^{-5}$  g/cm<sup>3</sup> per second (Case 2), a decrease of 52.1%. The dilutive played the most important role in the drop of inception rates, leading to a decrease of  $1.7 \cdot 10^{-5}$  g/cm<sup>3</sup> per second (35.4%) by comparison of maximum inception rates for Cases 1 and 4. The difference between the maximum inception rates in Cases 2 and 3 illustrated that the chemical effect of CO<sub>2</sub> had a significant suppression effect on the soot inception rate, with a decrease of  $0.7 \cdot 10^{-5}$  g/cm<sup>3</sup> per second (23.3%). However, the comparison between Cases 3 and 4 showed that the radiative effect of CO<sub>2</sub> on the soot inception rate can be ignored.

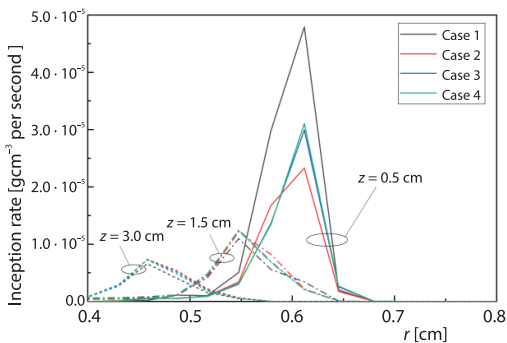


Figure 4. The radial profile of inception rate at heights of 0.5, 1.5, and 3.0 cm

The soot inception was modeled by the collision of two A4 in this study. The radial profile of mole fraction of A4 were depicted in fig. 5(b). It was clear that the A4 showed a similar profile with the inception rates at three heights for all cases. The dilutive and chemical

effects of CO<sub>2</sub> caused the 22.7% and 11.8% decrease in the maximum mole fraction of A4, less than those of inception rates (35.4% and 23.3%). That indicated the inception rate not only depended on the A4 mole fraction, but also on the temperature shown in fig. 2.

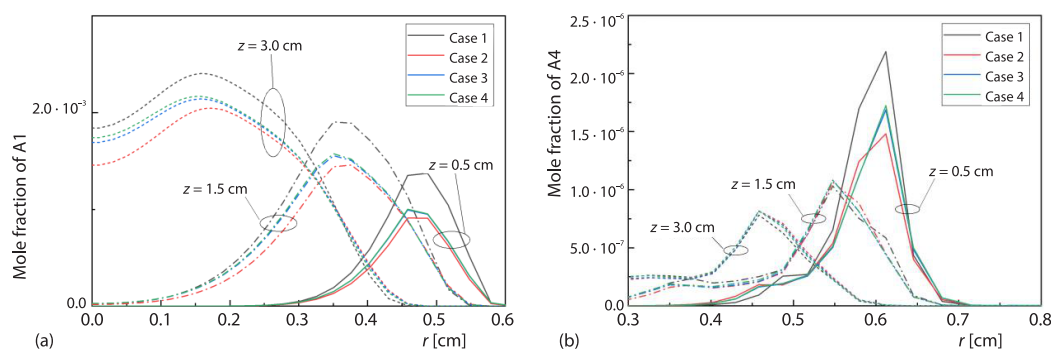


Figure 5. The radial profiles of mole fraction of A1 and A4 at heights of 0.5, 1.5, and 3.0 cm

The benzene (A1) was the first ring-structure species and dominated the formation of A4 [23]. The radial profile of mole fraction of A1 were depicted in fig. 5(a). It was shown that the maximum mole fraction of A1 increased and its location shifted to the centerline region as the height increasing. The CO<sub>2</sub> addition reduced the mole fraction of A1 at three different heights. Once again, the dilutive effect of CO<sub>2</sub> contributed the most effect on the decrease of mole fraction of A1, and the chemical effect of CO<sub>2</sub> was the secondary factor. The dilutive effect of CO<sub>2</sub> on the decrease of mole fraction of A1 could be explained by two reasons. One was the difference in heat capacity between CO<sub>2</sub> and air, which lowered the flame temperature, figs. 2(a) and 2(d), and consequently limited the reaction rates participating in the formations of PAH. The other one was the oxygen dilutive caused by the CO<sub>2</sub> addition. Decreasing oxygen concentration would suppressed the growth of PAH [6]. To further explain the chemical effect of CO<sub>2</sub> on the A1 formation, the integral reaction rates of reactions participating in A1 formation over the whole computational domain were calculated by:

$$\alpha = 2\pi \int_0^{\bar{z}} \int_0^r S r dr dz \quad (1)$$

where  $S$  was the reaction rate at the given location.

The A1 formation pathways were displayed in fig. 6 based on the  $\alpha$ s in Cases 2 and 3. It was clear that the A1 formation processes can be divided into two-stages: the decomposition of fuels into light hydrocarbons and the growth of light hydrocarbons to A1. For the C<sub>10</sub>H<sub>22</sub> and C<sub>9</sub>H<sub>18</sub>, the C<sub>2</sub>H<sub>4</sub> was the most important product which grew into the A1 through the pathway of C<sub>2</sub>H<sub>4</sub> → C<sub>2</sub>H<sub>3</sub> → C<sub>2</sub>H<sub>2</sub> → C<sub>2</sub>H → pC<sub>3</sub>H<sub>4</sub> → C<sub>3</sub>H<sub>3</sub> → C<sub>6</sub>H<sub>6</sub>. Another significant A1 formation mechanism was the H-addition reaction of C<sub>6</sub>H<sub>5</sub>, which was the main decomposition product of the C<sub>9</sub>H<sub>12</sub>.

The integral reaction rates for Cases 2 and 3 were compared in fig. 6 to investigate how the chemical effect of CO<sub>2</sub> affected the A1 formation. It was clear that the chemical effect of CO<sub>2</sub> reduced the  $\alpha$ R1421 (C<sub>6</sub>H<sub>5</sub> + H = C<sub>6</sub>H<sub>6</sub>) by 0.12 · 10<sup>-6</sup> mol/s (from 1.79 · 10<sup>-6</sup> to 1.62 · 10<sup>-6</sup> mol/s), which dominated on the decrease of A1 mole fraction. The yield of C<sub>6</sub>H<sub>5</sub> was mainly through the decomposition reaction of APHC2H4 (R1497:APHC2H4 = C<sub>6</sub>H<sub>5</sub> + C<sub>2</sub>H<sub>4</sub>). As shown in fig. 6, little discrepancy can be found between the  $\alpha$ R1497 in Cases 2 (1.81 · 10<sup>-6</sup> mol/s) and 3 (1.80 · 10<sup>-6</sup> mol/s). This implied the chemical effect of CO<sub>2</sub> on the C<sub>6</sub>H<sub>5</sub>

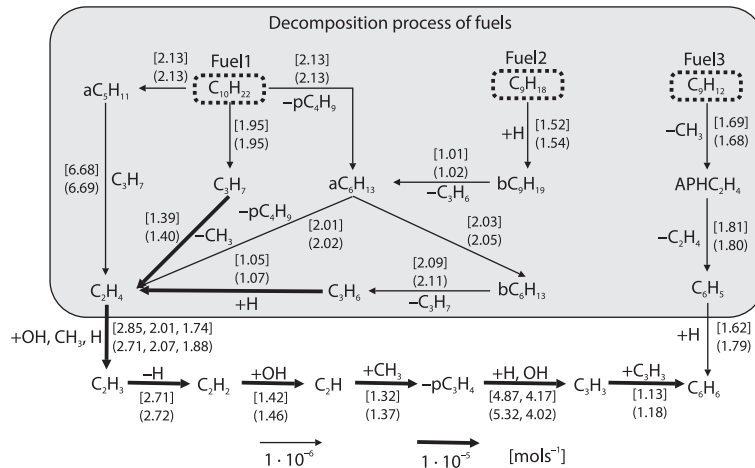


Figure 6. The formation pathways of A1, the values in square bracket and parenthesis indicate the integral rates for Cases 2 and 3, respectively

formation could be neglected, which demonstrated that C<sub>6</sub>H<sub>5</sub> was not the reason for the decrease of αR1421. The H radical was the other reactant in the R1421 and its radial profile of mole fraction at heights of 0.5, 1.5, and 3.0 cm were plotted in fig. 7(a). It was obvious that the H radical mole fractions at three heights in Case 2 less than those in Case 3. Hence, it can be concluded that the chemical effect of CO<sub>2</sub> decreased the H radical mole fraction, subsequently lowering the reaction rate of R1421, resulting in the decrease of the A1 mole fraction.

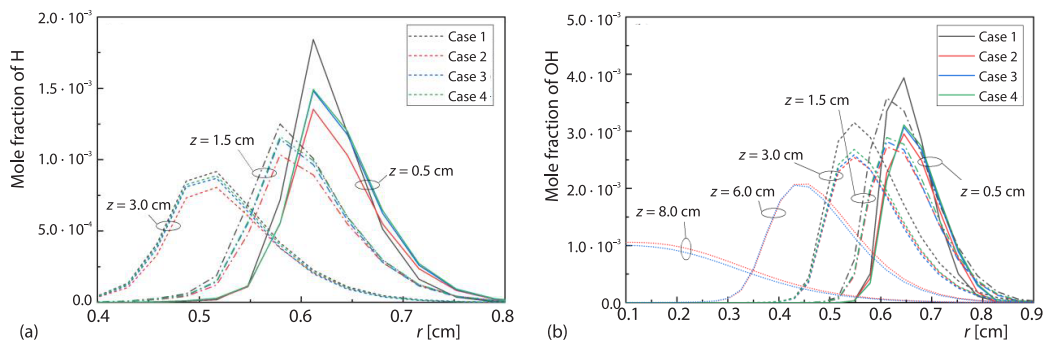


Figure 7. The radial profiles of mole fraction of H and OH at heights of 0.5, 1.5, and 3.0 cm

The decrease of αR230 (2C<sub>3</sub>H<sub>3</sub> = C<sub>6</sub>H<sub>6</sub>) by 0.05 · 10<sup>-6</sup> mol/s was the other factor contributing to the decrease of A1 mole fraction. There were two primary channels that contribute to the formation of C<sub>3</sub>H<sub>3</sub>. One was the H-abstraction reaction of pC<sub>3</sub>H<sub>4</sub> with H radical (R681: pC<sub>3</sub>H<sub>4</sub> + H = C<sub>3</sub>H<sub>3</sub> + H<sub>2</sub>). The other was the H-abstraction reaction of pC<sub>3</sub>H<sub>4</sub> with OH radical (R671: pC<sub>3</sub>H<sub>4</sub> + OH = C<sub>3</sub>H<sub>3</sub> + H<sub>2</sub>O). As manifested in fig. 6, the chemical effect of CO<sub>2</sub> resulted in a decrease of αR681 by 0.45 · 10<sup>-6</sup> mol/s, but an increase of αR671 by 0.15 · 10<sup>-6</sup> mol/s. As indicated in fig. 7(a), the decrease of H radical was responsible for the decrease of αR681. The radial profile of mole fraction of OH at heights of 0.5, 1.5, and 3.0 cm were depicted in fig. 7(b) to illustrate the increase of αR671. Surprisingly, the chemical effect of CO<sub>2</sub> reduced the OH mole fractions at heights of 0.5, 1.5, and 3.0 cm, which were inconsistent with the change of αR671. However, it can be observed in fig. 7(b) that the difference of OH mole

fraction between Cases 2 and 3 had become smaller as the height increased. The OH mole fraction in Case 2 was even a little larger than that in Case 3 at height of 3.0 cm where the radius was larger than 0.6 cm. Further, the radial profile of mole fraction of OH at heights of 6.0 and 8.0 cm for Cases 2 and 3 were also plotted in fig. 7(b). Obviously, the chemical effect of CO<sub>2</sub> caused an increase of OH mole fraction at heights of 6.0 and 8.0 cm. This demonstrated the increase of OH mole fraction at higher region of flame was the dominant role in the rise of  $\alpha R671$ .

The C<sub>2</sub>H<sub>4</sub>, as the key intermediate product of C<sub>10</sub>H<sub>22</sub> and C<sub>9</sub>H<sub>18</sub>, was the initial precursor for the A1 formation. As shown in fig. 6, the chemical effect of CO<sub>2</sub> did not affect the formation reactions of C<sub>2</sub>H<sub>4</sub>. That was mainly caused by the little difference in the decomposition processes of C<sub>10</sub>H<sub>22</sub> and C<sub>9</sub>H<sub>18</sub> between Cases 2 and 3. The yield of C<sub>2</sub>H<sub>3</sub> mainly through R419 (C<sub>2</sub>H<sub>4</sub> + OH = C<sub>2</sub>H<sub>3</sub> + H<sub>2</sub>O), R425 (C<sub>2</sub>H<sub>4</sub> + CH<sub>3</sub> = C<sub>2</sub>H<sub>3</sub> + CH<sub>4</sub>), and R422 (C<sub>2</sub>H<sub>4</sub> + H = C<sub>2</sub>H<sub>3</sub> + H<sub>2</sub>). The chemical effect of CO<sub>2</sub> increased the  $\alpha R419$  by  $0.14 \cdot 10^{-5}$  mol/s, but decreased the  $\alpha R425$  and  $\alpha R422$  by  $0.06 \cdot 10^{-5}$  and  $0.14 \cdot 10^{-5}$  mol/s. The decrease of formation rate of C<sub>2</sub>H<sub>3</sub> eventually limited the C<sub>6</sub>H<sub>6</sub> formation through C<sub>2</sub>H<sub>3</sub> → C<sub>2</sub>H<sub>2</sub> → C<sub>2</sub>H → pC<sub>3</sub>H<sub>4</sub> → C<sub>3</sub>H<sub>3</sub> → C<sub>6</sub>H<sub>6</sub>.

In general, the chemical effect of CO<sub>2</sub> caused little difference in the decomposition processes of C<sub>10</sub>H<sub>22</sub>, C<sub>9</sub>H<sub>18</sub>, and C<sub>9</sub>H<sub>12</sub>. The decrease of H mole fraction caused by the chemical effect of CO<sub>2</sub> resulted in the decrease of A1 mole fraction through R1421. The decrease of  $\alpha R230$  was the other factor contributing to the decrease of A1 mole fraction, which was initially caused by the decrease of C<sub>2</sub>H<sub>3</sub> formation through R422 and R425.

#### The effect of CO<sub>2</sub> on soot condensation and HACA surface growth

The different effects of CO<sub>2</sub> addition on the soot condensation rate at heights of 0.5, 1.5, and 3.0 cm were plotted in fig. 8(a). Unlike the soot inception, the soot condensation rates at heights of 1.5 and 3.0 cm were higher than those at 0.5 cm. This implied the soot condensation happened at a higher region of the flame. Comparing Cases 1 and 2, the CO<sub>2</sub> addition dramatically limited the soot condensation at three different heights. At height of 3.0 cm, the dilutive effect of CO<sub>2</sub> lowered the maximum soot condensation rate by 42.1% (from  $2.90 \cdot 10^{-4}$  to  $1.68 \cdot 10^{-4}$  g/cm<sup>3</sup> per second), comparing Cases 1 and 4. The chemical and radiative effect of CO<sub>2</sub> showed a similar ability to suppress the soot condensation. The chemical effect of CO<sub>2</sub> decreased the maximum soot condensation rate at height of 3.0 cm by 8.4% (from  $1.55 \cdot 10^{-4}$  to  $1.42 \cdot 10^{-4}$  g/cm<sup>3</sup> per second), which was larger than the radiative effect of CO<sub>2</sub> (by 7.7%, from  $1.68 \cdot 10^{-4}$  to  $1.55 \cdot 10^{-4}$  g/cm<sup>3</sup> per second). The condensation process was modeled by the collision between the soot and A4. Thus, it depended on the temperature and the mole fraction of soot and A4. As discussed in section 5.2, the chemical and radiative effect of CO<sub>2</sub> lowered the temperature,

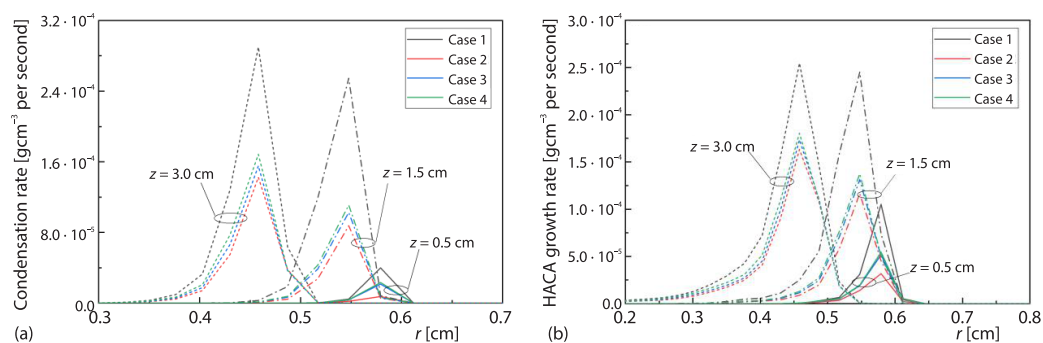


Figure 8. The radial profiles of condensation and HACA growth rates at heights of 0.5, 1.5, and 3.0 cm

leading to the decrease of soot condensation. The soot inception was the first process in the soot formation and providing the precursor (soot) for the condensation process. The soot inception was limited by the chemical effect of CO<sub>2</sub>, but little limited by the radiative effect of CO<sub>2</sub>, see fig. 4. This illustrated that the chemical effect of CO<sub>2</sub> (8.4%) had a more dramatic impact on the soot condensation than the radiative effect of CO<sub>2</sub> (7.7%).

The different effects of CO<sub>2</sub> addition on the HACA growth rates at heights of 0.5, 1.5, and 3.0 cm were plotted in fig. 8(b). Similar to the soot condensation, the CO<sub>2</sub> addition dramatically suppressed the HACA growth rate. The dilutive effect of CO<sub>2</sub> contributed the most effect on the decrease of the HACA growth rate, followed by the chemical effect of CO<sub>2</sub>, but the radiative effect of CO<sub>2</sub> was small.

### Conclusions

The effects of CO<sub>2</sub> addition the air-flow on the laminar co-flow Jet A-1 kerosene diffusion flame were numerically studied by employing detailed soot sectional models and a detailed chemical mechanism. Four different cases were investigated to isolate the dilutive, chemical and radiative effects of CO<sub>2</sub> on the soot inception, condensation and HACA growth rates. Following were the main conclusions.

- The addition of 15 vol.% CO<sub>2</sub> had a significant suppression effect on the temperature and soot formation. It dramatically decreased the peak temperature by 92 K and decreased the maximum soot mole fraction by 41.0% (from 2.90-1.71 ppm).
- The dilutive effect of CO<sub>2</sub> contributed the most effect on the decrease of temperature and soot mole fraction. Moreover, it was the main factor in the decrease of soot inception, soot condensation and HACA growth rates. The chemical effect of CO<sub>2</sub> was the secondary factor.
- The chemical effect of CO<sub>2</sub> had little influence on the decomposition of fuels into light hydrocarbons, but obviously limited the growth of light hydrocarbons to A1.
- The radiative effect of CO<sub>2</sub> decreased the maximum temperature and soot mole fraction by 13 K and 5.2% (from 1.92-1.82 ppm), respectively. It had little impact on the soot inception, soot condensation and HACA growth rates.

### Acknowledgment

This work was supported by the National Natural Science Foundation of China (No. 51976057).

### Author's contribution

Yang, Y., and Li, Q., are co-first authors and contributed equally to the work.

### Nomenclature

$f_v$  – the soot volume fraction, [–]

$h$  – height, [cm]

$r$  – radius, [mm]

$S$  – reaction rate at the given location, [molcm<sup>-3</sup> per second]

*Greek symbol*

$\alpha$  – the integral reaction rate over the whole computational domain, [mols<sup>-1</sup>]

*Acronyms*

DOM – discrete ordinate method

SVF – soot volume fraction

### References

- [1] Zhao, T., *et al.*, The Evolution of Soot Morphology for the Maturation of Nascent Particle in a Turbulent Lifted Jet Flame, *Thermal Science*, 26 (2022), 6A, pp. 4595-4605

- [2] Wang, Y., Chung, S. H., Soot Formation in Laminar Counterflow Flames, *Progress in Energy and Combustion Science*, 74 (2019), Sept., pp. 152-238
- [3] Feng, R., et al., Ignition and Combustion Enhancement in a Cavity-Based Supersonic Combustor by a Multi-Channel Gliding Arc Plasma, *Experimental Thermal and Fluid Science*, 120 (2021), 110248
- [4] Feng, R., et al., Suppression of Combustion Mode Transitions in a Hydrogen-Fueled Scramjet Combustor by a Multi-Channel Gliding Arc Plasma, *Combustion and Flame*, 237 (2022), 111843
- [5] Ju, H., et al., Modelling of Soot Particle collision and Growth paths in Gas-solid Two-phase flow, *Thermal Science*, 25 (2021), 5B, pp. 3741-3752
- [6] Jerez, A., et al., Soot Production Modelling in a Laminar Coflow Ethylene Diffusion Flame at Different Oxygen Indices Using a PAH-Based Sectional Model, *Fuel*, 231 (2018), Nov., pp. 404-416
- [7] Sun, M., et al., Numerical and Experimental Investigation of Soot Precursor and Primary Particle Size of Aviation Fuel (RP-3) and n-Dodecane in Laminar Flame, *Journal of the Energy Institute*, 94 (2021), Feb., pp. 49-62
- [8] Saffaripour, M., et al., Experimental Investigation and Detailed Modelling of Soot Aggregate Formation and Size Distribution in Laminar Coflow Diffusion Flames of Jet A-1, A Synthetic Kerosene, and n-Decane, *Combustion and Flame*, 161 (2014), 3, pp. 848-863.
- [9] Sun, M., et al., Comparison Study of Soot Precursor and Aggregate Property Between Algae-Based Aviation Biofuel and Aviation Kerosene RP-3 in Laminar Flame, *Journal of Energy Resources Technology*, 143 (2021), 11
- [10] Abdalla, A. O., et al., Soot Formation and Evolution in RP-3 Kerosene Inverse Diffusion Flames: Effects of Flow Rates and Dimethyl Carbonate Additions, *Fuel*, 273 (2020), 117732
- [11] Sui, R., et al., Kinetic Modelling of Total Oxidation of Propane over Rhodium, *Combustion and Flame*, (2021), 111847
- [12] Choubey, G., et al., Hydrogen Fuel in Scramjet Engines-A Brief Review, *International Journal of Hydrogen Energy*, 45 (2020), 33, pp. 16799-16815
- [13] Zheng, S., et al., Effects of Radiation Reabsorption on the Laminar Flame Speed and NO Emission during Aviation Kerosene Combustion at Elevated Pressures, *Fuel*, 324 (2022), 124545
- [14] Pellett, G., et al., Review of Air Vitiation Effects on Scramjet Ignition and Flameholding Combustion *Proceedings*, 38<sup>th</sup> AIAA/ASME/SAE/ASEE Joint Propulsion Conference and Exhibit, Indianapolis, Ind. USA, 2002
- [15] Liang, J.-H., et al., The Vitiation Effects of Water Vapor and Carbon Dioxide on the Autoignition Characteristics of Kerosene, *Acta Mechanica Sinica*, 30 (2014), 4, pp. 485-494
- [16] Wang, Y., et al., Experimental Study of Vitiation Effects on Hydrogen/Kerosene Fueled Supersonic Combustor, *Aerospace Science and Technology*, 60 (2017), Jan., pp. 108-114
- [17] Li, J., et al., Numerical Investigation of H<sub>2</sub>O and CO<sub>2</sub> Vitiation Effects on Kerosene-Fueled Supersonic Combustion, *Journal of Propulsion Technology*, 34 (2013), 4, pp. 563-571
- [18] Samanta, A., et al., Effect of CO<sub>2</sub> Dilution on Flame Structure and Soot and NO Formations in CH<sub>4</sub>-Air Non-Premixed Flames, *Journal of Engineering for Gas Turbines and Power*, 132 (2010), 12
- [19] Guo, H., Smallwood, G. J., A Numerical Study on the Influence of CO<sub>2</sub> Addition on Soot Formation in an Ethylene/Air Diffusion Flame, *Combustion Science and Technology*, 180 (2008), 10-11, pp. 1695-1708
- [20] Liu, F., et al., The Chemical Effect of CO<sub>2</sub> Replacement of N<sub>2</sub> in Air on the Burning Velocity of CH<sub>4</sub> and H<sub>2</sub> Premixed Flames, *Combustion and Flame*, 133 (2003), 4, pp. 495-497
- [21] Zheng, S., et al., Effects of C<sub>2</sub>H<sub>2</sub> and C<sub>2</sub>H<sub>4</sub> Radiation on Soot Formation in Ethylene/Air Diffusion Flames, *Applied Thermal Engineering*, 183 (2021), 116194
- [22] Zheng, et al., Effects of Radiation Reabsorption on the Laminar Burning Velocity of Methane/Air and Methane/Hydrogen/Air Flames at Elevated Pressures, *Fuel*, 311 (2022), 122586
- [23] Liu, F., et al., Effects of Water Vapor Addition the Air Stream on Soot Formation and Flame Properties in a Laminar Coflow Ethylene/Air Diffusion Flame, *Combustion and Flame*, 161 (2014), 7, pp. 1724-1734
- [24] Riviere, P., Soufiani, A., Updated Band Model Parameters for H<sub>2</sub>O, CO<sub>2</sub>, CH<sub>4</sub>, and CO Radiation at High Temperature, *International Journal of Heat and Mass Transfer*, 55 (2012), 13-14, pp. 3349-3358
- [25] Eaves, N. A., et al., CoFlame: A Refined and Validated Numerical Algorithm for Modelling Sooting Laminar Coflow Diffusion Flames, *Computer Physics Communications*, 207 (2016), Oct., pp. 464-477
- [26] Wei, M., et al., Effects of Ethanol Addition on Soot Particles Dynamic Evolution in Ethylene/Air Laminar Premixed Flame, *Thermal Science*, 22 (2018), 3, pp. 1339-1350
- [27] Liu, F., et al., Effects of Radiation Model on the Modelling of a Laminar Coflow Methane/Air Diffusion Flame, *Combustion and Flame*, 138 (2004), 1-2, pp. 136-154

- [28] Thurgood, C., *et al.*, The TN Quadrature Set for the Discrete Ordinates Method, *Journal of Heat Transfer*, 117 (1995), 4, pp. 1068-1070
- [29] Zhang, C., *et al.*, Effects of Soot Inception and Condensation PAH Species and Fuel Preheating on Soot Formation Modelling in Laminar Coflow CH<sub>4</sub>/Air Diffusion Flames Doped with n-Heptane/Toluene Mixtures, *Fuel*, 253 (2019), Oct., pp. 1371-1377